Observation of stable marine boundary layer by shipborne Coherent Doppler Lidar and radiosonde over Yellow Sea

ZHAI Xiaochun[1, 2], WU Songhua[1, 3], LIU Bingyi[1, 3], YIN Jiaping[4], ZHANG Hongwei[1]

1. *Deutsches Zentrum für Luft- und Raumfahrt.V. (DLR), Institut für Physik der Atmosphäre, Oberpfaffenhofen* 82234*, Germany*;
2. *Ocean Remote Sensing Institute, Ocean University of China, Qingdao* 266100*, China*;
3. *Laboratory for Regional Oceanography and Numerical Modeling, Qingdao National Laboratory for Marine Science and Technology, Qingdao* 266100*, China*;
4. *Qingdao Leice Transient Technology Ltd., Qingdao* 266100*, China*

Abstract: Shipborne observations obtained with the Coherent Doppler lidar (CDL) and radiosonde during 2014 campaign were used to study the structure of marine boundary layer in Yellow Sea. Vertical wind profiles corrected for ship motion was used to derive higher-order statistics, showing that motion correction is required and significant for turbulence analysis. During a day with weak mesoscale activity, a complexed three-layer structure system was observed. The lowest layer showed a typical stable boundary layer structure feature. An aerosol layer with abrupt variation in wind speed and relative humidity always appeared at the middle layer, the formation of which may be due to Kelvin-Helmholz instability. The top layer encountered a dramatic change in wind direction, which may result from the warm advection from the Eurasian continent on the basis of backward trajectory analysis. Furthermore, the MABL height in stable regime was derived from potential temperature, CDL Signal-to-Noise Ratio (SNR) and CDL vertical velocity variance, respectively. The Stable Boundary Layer (SBL) height in SBL can be derived from the inversion layer of potential temperature profile, and the mixing height in SBL can be retrieved from the vertical velocity variance gradient method. Neither the SBL height nor the mixing height is in agreement with the height retrieved from CDL SNR gradient method because of different definition and criterion. One of the limitations of SNR gradient method for MABL retrieval is that it is easier to be affected by the lofted decoupled aerosol layer, where the retrieved result is less suitable. Finally, the higher-order vertical velocity statistics within the marine stable boundary layer were investigated and compared with the previous studies, and different turbulence mechanisms have an important effect on the statistics deviation.

Key words: coherent Doppler Lidar, stable marine boundary layer, radiosonde, turbulence characteristics

Citation format: **Zhai X C,Wu S H,Liu B Y,Yin J P and Zhang H W. 2020. Observation of stable marine boundary layer by shipborne Coherent Doppler Lidar and radiosonde over Yellow Sea. Journal of Remote Sensing(Chinese). 24(S1): 76−88**

1 INTRODUCTION

Marine Atmospheric Boundary Layer (MABL) is the connection between sea surface and free atmosphere. The vertical structure of the atmospheric variables in the MABL plays a significant role in the matter-energy interaction at the air-sea interface, the development of clouds at the top of the MABL and the transport, lifetimes, and diurnal cycles of aerosol and gaseous trace species. Conventional MABL measuring methods such as buoy, wind tower, radiosonde and weather radar are difficult to provide high-precision wind velocity, especially vertical velocity, which is demanding for the measurement of air-sea boundary layer turbulence flux (Mitsuta, et al., 1974, Hawley, et al., 1993). In recent year, considerable progress has been made in the development, improvement and application of active remote sensing system for MABL research. Coherent Doppler lidar (CDL) is an available tool with high spatial and temporal resolution, providing nearly continuous particle backscatter, wind profile observations in the clear atmosphere. There has been extensive research on MABL structure using CDL. Eberhard, et al. (1989) estimated the vertical profiles of the variance of wind velocity and the momentum flux retrieved from wind data measured by pulsed CDL. Shipborne observations obtained with the NOAA high resolution Doppler lidar (HRDL) were used to study the convective MABL in the tropical Pacific Ocean (Wulfmeyer, et al., 2005). Profiles of mean winds and turbulence were measured by HRDL in the strong-wind stable boundary layer (Ban-

---

Received: XXXX-XX-XX; **Accepted:** XXXX-XX-XX

Foundation: National Key R&D Program of China (No. 2016YFC1400904; ESA-MOST Dragon 4 Cooperation (No. 32296); National Natural Science Foundation of China (No. 41471309; 41375016)

First author biography: ZHAI Xiaochun (1992—), female, Ocean University of China, atmospheric dynamics and turbulence E-mail: zhaixiaochun@163.com

Corresponding author biography: WU Songhua (1976—), male, Ocean University of China, laser technique and remote sensing E-mail: wush@ouc.edu.cn

ta, et al., 2006). Tucker et. al. (Tucker, et al., 2009) estimated the marine mixing height using turbulence, shear, and aerosol profiles based on Doppler lidar during TexAQS 2006 campaign.

Properties of the surface over which the boundary layer forms can affect the stability and thus the measurements made in this layer. The radiative-driven, stable boundary layer over land has been the focus of a large number of theoretical and observational studies, however, there have been a few detailed measurements of Stable Marine Boundary Layer (SMBL) over the ocean, especially the work on the offshore problem in terms of warm air flowing out over a colder sea. Its importance should not be underestimated since air over the cool coastal ocean is often close to neutral or slightly stable. The stable internal boundary layers over a cold sea were first studied by Csanady, et al., (1974). Garratt, et al, (1987) applied a numerical model on aircraft data off the Australian coast to show that the internal boundary layer can be characterized by a critical layer-flux Richardson number. Smedman, et al., (1997) used a two-dimensional numerical model together with measurements to study the SMBL over the Baltic Sea and found that stratification was always stable in the air layers near the sea surface. Rogers, et al., (1996) used the aircraft data to study the turbulence structure at the upwind and downwind ends of a coastal area and found that stable layers were frequent features of the coastal MABL. Angevine, et al., (2006) explored how the SMBL was formed over the Gulf of Maine.

This paper introduces the experimental investigation which was carried out to measure the wind field and turbulence characteristics of MABL of the Yellow Sea and the Bohai Gulf by CDL in 2014. The operation of CDL on a research vessel is an important test of the reliability of such a delicate system. In section 2, the specific experimental campaign and CDL performance mode are described in detail. An analysis of a 16-h time series is presented in Section 3 and 4, covering the period from 2300 UTC May 8, 2014 to 1400 UTC May 9, 2014. During this observation period, the SMBL structure and formation are presented and analyzed using National Center for Environmental Prediction (NCEP) reanalysis, radiosonde and CDL data, including the stability, horizontal and vertical velocity profiles, MABL height, turbulence statistics and so forth. Comparison of these results with previous measurements are also presented. The conclusions are given in Section 5.

2 EXPERIMENT AND CDL SETUP

This field project was undertaken by Dongfanghong-2 research vessel affiliated with Ocean University of China (OUC) to investigate the MABL characteristics of the Yellow Sea and Bohai Gulf (32°N—40°N,118.5°E—125.3°E). The Yellow Sea is the northern part of the East China Sea, which is a marginal sea of the Pacific Ocean. It is located between mainland China and the Korean Peninsula, which is linked with the Bohai Sea, the innermost gulf of the Yellow Sea on the coast of Northeastern and North China by Bohai Strait. The experimental campaign was divided into two voyages. The first voyage set out on 27 April 2014 from Qingdao to carry out the research in South Yellow Sea, and then returned to Qingdao on 7 May 2014. After a day of replenishment, the second voyage continued to visit the northern Yellow Sea and Bohai sea, and finally returned to Qingdao port on May 18, 2014. The blue dotted line in Fig. 1 shows the specific experimental shipping line. The voyage location analyzed in this paper is marked with red line. As can be seen in Fig. 1, the closest distance between the measurement site (red line) to the shore is about 180 km, where the folding of internal boundary layer plays minor role on the atmospheric condition during the analyzed observational period.

One of the goals of this campaign is to improve our understanding of MABL dynamic and thermal characteristics, turbulence and entrainment in the mid-latitude oceanic area. During this campaign, observations were collected using CDL, Vaisala commercial CL31 ceilometer and radiosondes. These instruments were located at the high second deck to avoid the disturbance of barrier. The whole voyage released 32 radiosonde balloons, 27 of which was measured in sunny conditions and five datasets were obtained in the rain, fog, and cloudy conditions. The CDL is supplied by the OUC Ocean Remote Sensing Institute (ORSI) to make high-resolution wind and aerosol particle measurements during this campaign (Wu, et al., 2016, Zhai, et al., 2018). It is located at the back of the upper deck and is around 8 m from the sea surface. The blind area of CDL is 120 m. The CDL is based on the heterodyne technique, and mainly consists of a single frequency fiber seed laser source operating on an eye-safe wavelength of $1.55\mu m$, a high-speed scanner permitting 3D measurements of atmospheric variables, a balanced detector and FFT signal processor. The complete system is transportable in a single container. The detection range of 4000 m (maximum 6000 m at a proper aerosol concentration) enables the system to monitor the complete MABL structure most of the time. The highlights of the CDL includes the flexible range resolution from 15 m to 60 m and relatively high sampling rate, which is useful for detection of small -scale turbulence feature and reduces the uncertainty in an averaged wind measurement.

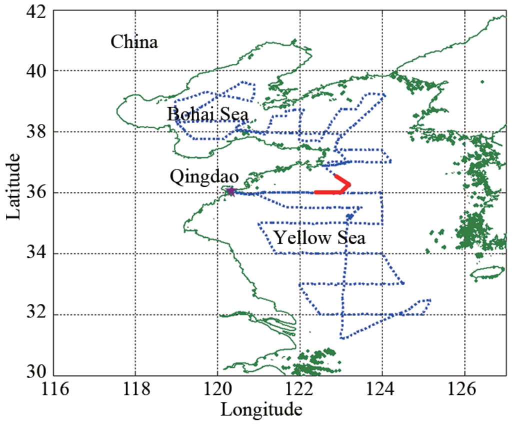

Fig.1 Cruise map of research vessel Dongfanghong-2 in the Yellow and Bohai Sea during 2014

Ship motion turns out to be an important error source for the determination of turbulence variables using CDL (Wulfmeyer, et al., 2005), therefore the motion correction should be considered before further analysis. The specific description of ship motion correction processing can be found in literature (Zhai, et al., 2018). Generally, in order to acquire the speed, position and attitude angles including the platform roll, pitch, and yaw data of the vessel during movement, a two-antenna differential GPS and an inertial navigation are installed on the ship-mounted CDL shown in Fig. 2. The inertial navigation system is fixed on the base of the scanner to keep constant relative angles with reference to the transmitting laser beam. After installation, a calibration is performed to determine the initial orientation of the laser beam.

CDL takes advantage of the fact that the frequency of the echo signal is shifted compared to the local-oscillator light because of the Doppler effect which occurs from backscattering of aerosols. The Doppler shift in the frequency of the backscattered signal is analyzed to obtain the radial velocity or Line-Of-Sight (LOS) velocity along the lidar beam direction. The lidar Signal-to-Noise-Ratio (SNR) derived from echo spectrum signal can be processed to estimate the relative intensity of the backscatter signal. For the application presented in this paper, the strength of SNR profiles from zenith stare periods can still be used to detect the aerosol gradient and thus retrieve the MABL height in spite of no correction. The LOS velocity and SNR are stored with a resolution of 30 m and 1 s, respectively. For studying the MABL height by SNR profiles and the horizontal wind profiles, 1min is required for reducing noise errors.

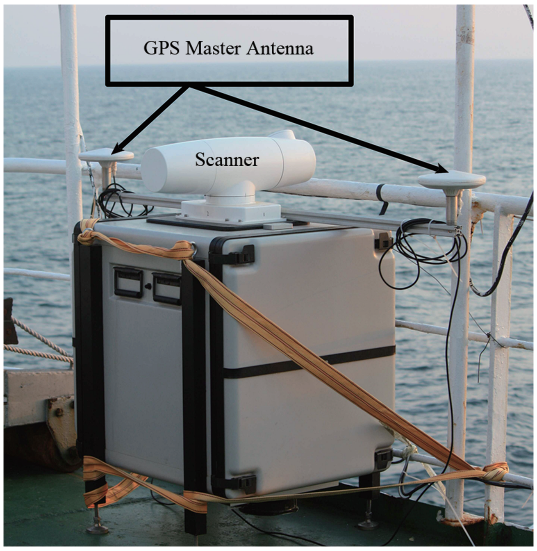

Fig.2 The Coherent Doppler Lidar (CDL) setup on Dongfanghong-2 research vessel

CDL collects a large set of data in three different operation modes. Mode 1 is called 4-Doppler-Beam-Swing (4-DBS) mode with changing azimuth angle of probing beam (0°-90°-180°-270°) at the fixed elevation angle to retrieve the horizontal wind profile. Mode 2 is the vertical pointing mode to get the vertical velocity and SNR. Furthermore, Velocity-Azimuth-Display (VAD) scanning mode (Strauch, et al., 1984) are performed at the elevation of 0°, 0.5°, 1.0°, 1.5°, 2.0° with a scan speed of 2 (°/s), which is called mode 3. Using mode 3, the sea surface and low levels wind can be derived with higher resolution, offering opportunity to further analyze the flux and turbulence characteristics in the air-sea interface. The homogeneity of the atmosphere over the ocean is assumed in mode 1 and 3. In this study, the focus is on measurement performed in mode 1 and 2.

3 INVESTIGATION OF STABLE BOUNDARY LAYER FORMATION

3.1 Weather situation and background data

During the field campaign, mainly fair-weather conditions are present. Except for a few showers (3 days) or fog (2 days) weather condition, the weather is mostly clear with some stratocumulus and high-level cirrus clouds. During the observational period from 07:00 local standard time (LST, UTC+8h) 9 May until 21:00 LST 9 May 2014 which will be further analyzed, a high-pressure system is close to the measurement site.

To describe the meteorological situation at the measurement site in detail, the surface and radiosonde data are analyzed shown in Fig. 3 and Fig. 4, respectively. The parameters shown in Fig. 3 are obtained from shipborne equipment. It can be seen that the surface horizontal wind speed varies between 0.05 m/s and 5.99 m/s with maximum at around 10:00 LST. The wind direction gradually shifted from northwest to East. Both the surface pressure and humidity have little diurnal variations with mean values of 1015 hPa and 89%, respectively. The surface sensible and latent heat flux shown in Fig. 4 are obtained from National Centers for Environmental Prediction (NCEP). The mean sensible heat flux is about -2.3 W/m^2 with standard deviation of 1.4 W/m^2. The negative sensible heat flux during the analyzed observation period (marked with red squares in Fig. 4 (a)) implies that a stable boundary layer (SBL) is present. The mean latent heat flux is about 8.8 W/m^2, varying between 2.4 W/m^2 and 16.4 W/m^2. The time series of surface sensible and latent heat fluxes show slight diurnal variations with maximum at daytime and minimum at nighttime. The Sea Surface Temperature (SST) and Surface Air Temperature (SAT) at the height of about 4 m are obtained from shipborne equipment and radiosonde data, respectively. Since the SAT can only be determined when the radiosonde data is available, 6 specific time point results are shown in Fig. 4 ranging from 13.7 ℃ to 14.9 ℃. The generally negative sea-air temperature difference is consistent with the negative sensible heat flux, suggesting that the stable stratification with weak turbulence transportation between sea surface and atmosphere occurs.

The radiosonde profiles of potential temperature, relative humidity and horizontal wind are available from 0805 LST 9 May until 1900 LST 9 May at about every two hours. Fig. 5 and Fig. 6 show the meteorological information obtained from radiosonde dataset at 08:05, 10:18 and 12:04 LST 9 May 2014, respectively. The profile of potential temperature shows a typical SBL structure feature which is shaded with yellow color (Stull, 2012), that is, an obvious inversion layer appears at the lower part of MABL, consistent with the negative sensible heat flux and negative sea-air temperature difference. The top of inversion layer is regarded as the SBL height in this situation (Liu, et al., 2010). It can be seen that the SBL height in all cases is less than 0.3 km with no distinct diurnal variation, showing the solar radiation is not the primary factor of turbulence development in this case. Furthermore, it is obvious from the potential temperature profile that the second inversion layer appears at around 1.5 km, as shown in Fig. 5 with blue color shaded area . The capping temperature inversion is not concentrated in a narrow region but is fairly deep. Below and above the second inversion layer, the potential temperature follows a nearly dry adiabatic lapse rate. At around the height of 2.3—2.8 km with purple color shaded area, the relative humidity increased obviously and is regarded as the third distinct layer. Generally, three distinct layers are detected by the in-situ radiosonde data, which will be analyzed in the following section. The relative humidity below SBL height decreases rapidly with height. One of the reasons is that the weak turbulence within SBL results in inadequate air mixing. Furthermore, the fluctuation of relative humidity profile above the SBL height shows the existence of multilevel aerosol layers, which can be shown more intuitively in the following wind profiles.

The profiles of horizontal wind speed (black lines) and wind direction (blue lines) are presented in Fig. 6, respectively. It is obviously shown that the wind direction changes dramatically from easterly wind below 1.5 km to the westerly wind above 1.5 km, while the wind speed follows a relatively smooth transition with height, implying that different air mass motions at different height ranges may occur in this condition. Furthermore, there is a disturbance in wind speed between 0.8 km and 1.5 km at all time period, consistent with the distinct feature of relative humidity profiles. The low-level jet near the SBL height are observed in all cases as well. It may be due to a sudden transition of the air flow from warm land surface to cold oceanic surface, causing an inertial oscillation of the horizontal wind vector because of the sudden disappearance of the retarding friction in the equilibrium of forces (Emeis, et al., 2012).

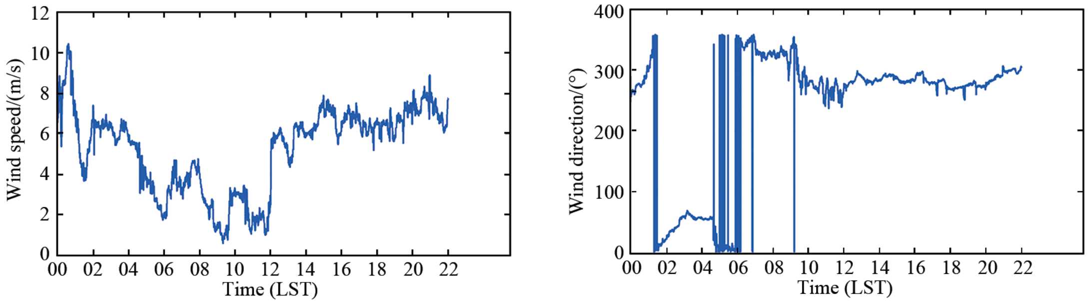

(a) Surface wind speed (b) wind direction

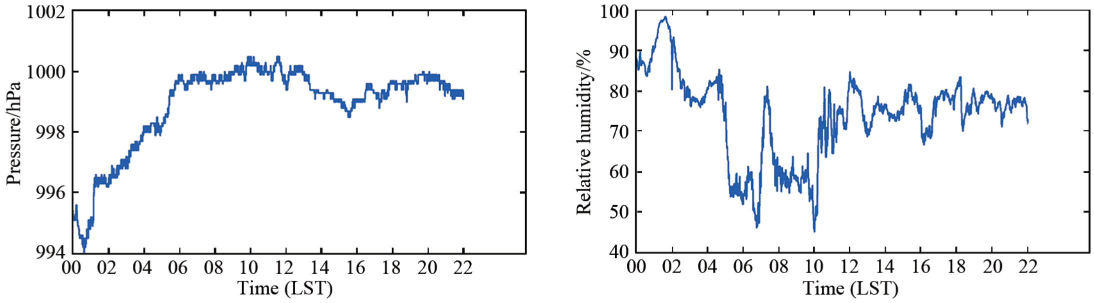

(c) pressure (d) relative humidity

Fig.3 Surface wind speed, wind direction, pressure and relative humidity during 8 and 9 May 2014 at corresponding voyage locations

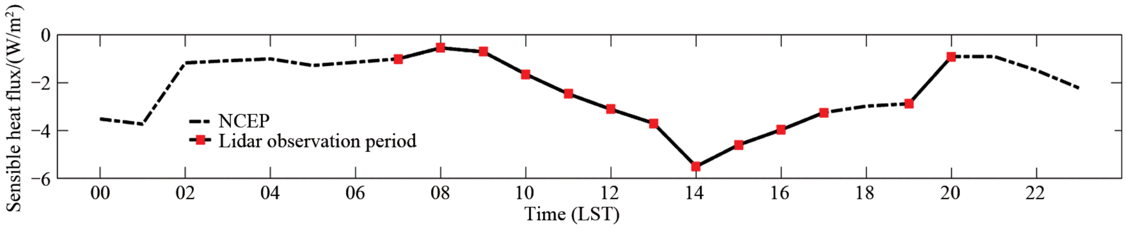

(a) Sensible heat flux

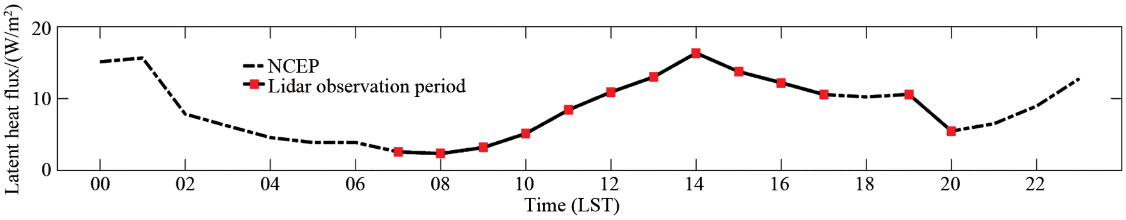

(b) latent heat flux

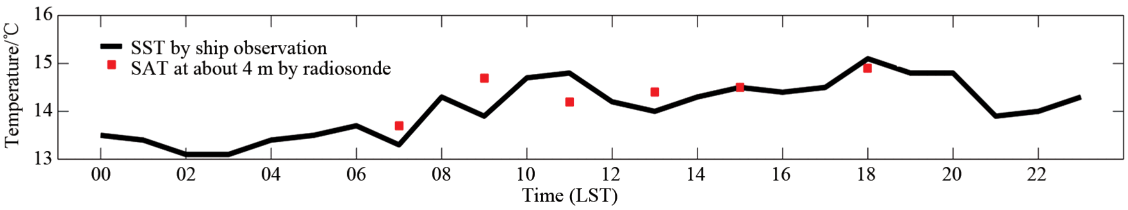

(c) sea surface temperature

Fig.4 Sensible heat flux and latent heat flux at corresponding voyage locations obtained from NCEP, the Lidar observation period is marked with red squares sea surface temperature obtained from ship equipment observation and surface air temperature at the height of about 4 m obtained from radiosonde dataset on 9 May 2014

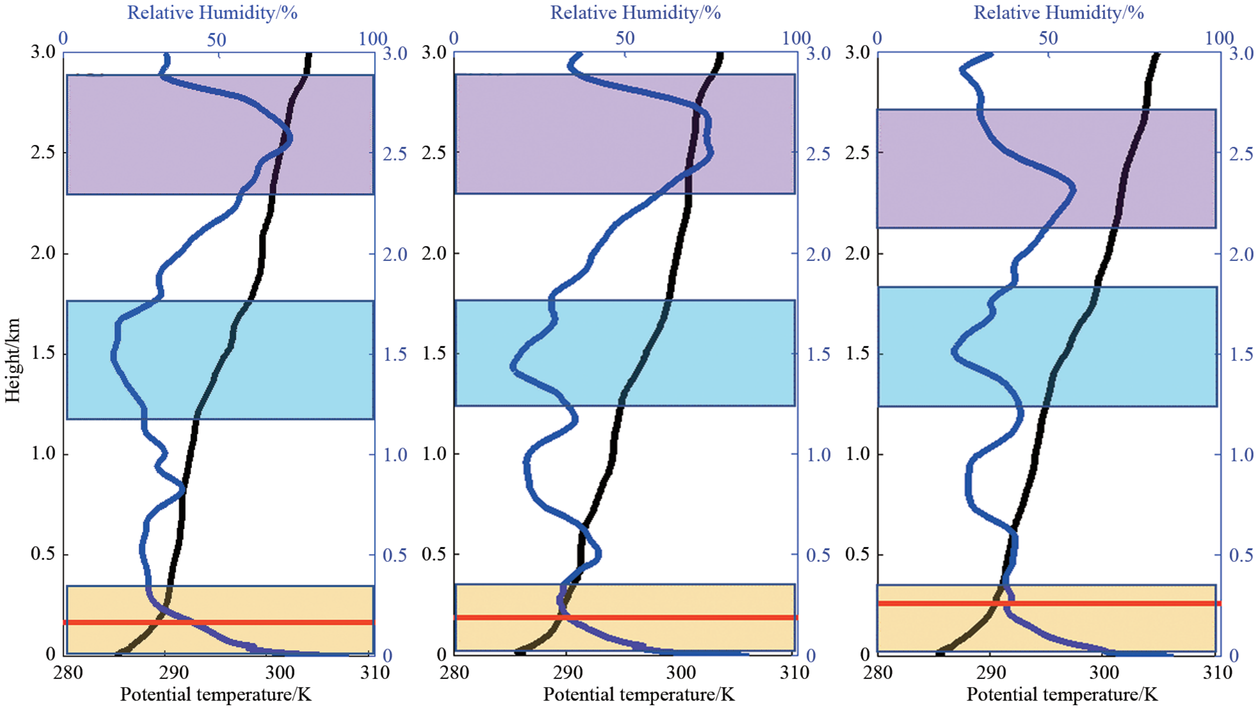

(a) 08:05 LST May 9, 2014 (b) 10:18 LST May 9, 2014 (c) 12:04 LST May 9, 2014

Fig.5 Radiosonde profiles of potential temperature (K, black line) and relative humidity (%, blue line) for (a) 08:05, (b) 10:18 and (c) 12:04 LST May 9, 2014 at corresponding voyage location, respectively, and the horizontal red lines are the SBL heights derived from the potential temperature characterization.

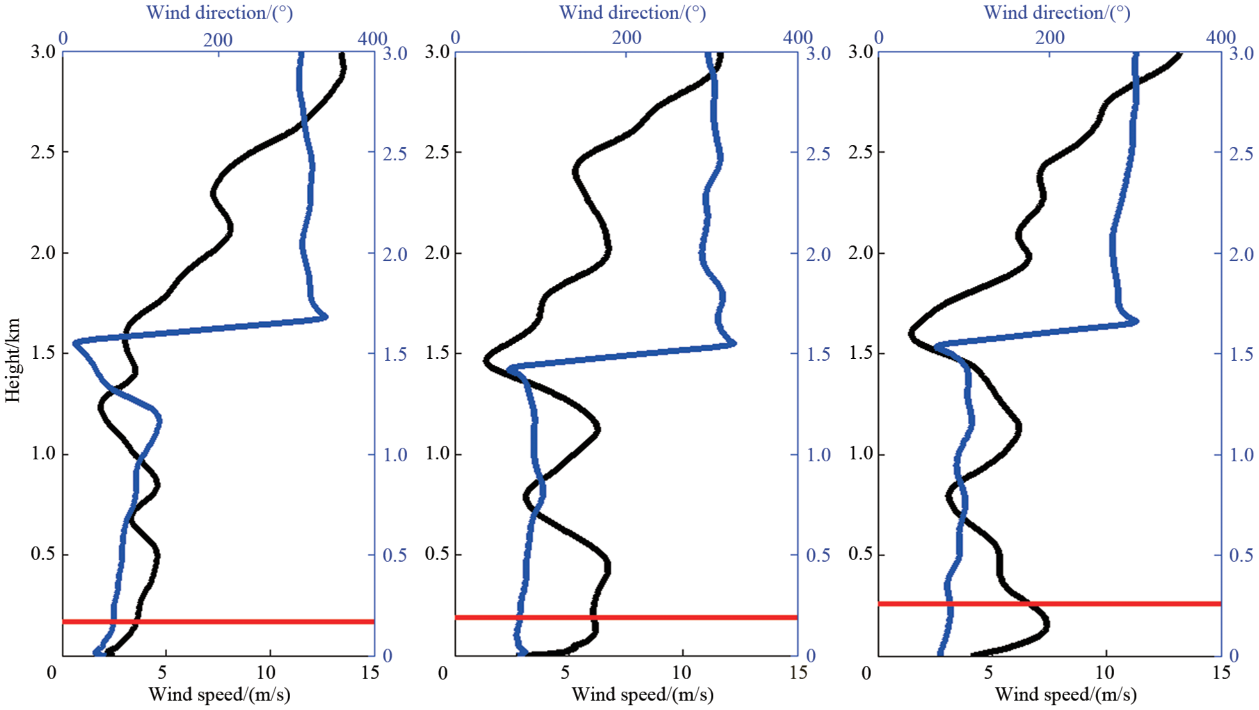

(a) 08:05 LST May 9, 2014 (b) 10:18 LST May 9, 2014 (c) 12:04 LST May 9, 2014

Fig.6 Radiosonde profiles of wind speed and direction at 08:05, 10:18 and 12:04 LST May 9 2014 at corresponding voyage location, respectively, and the horizontal red lines are the SBL height derived from potential temperature characterization

3.2 Wind shear and stability

The SBL turbulence can result from two dominant mechanisms: buoyancy forced and/or shear driven. The vertical wind shear can be calculated:

$$windshear = \sqrt{(\Delta U)^2 + (\Delta V)^2} / \Delta z \tag{1}$$

where ΔU and ΔV are horizontal velocity component differences at two orthogonal directions obtained over height difference $\Delta z = 10m$, respectively.

The profiles of vertical wind shear are presented in Fig. 7 with blue lines. It can be seen that strong wind shear occurs in the SBL because of the dramatic changes of horizontal wind speed. In this case, atmospheric turbulence is sustained by the presence of mechanical turbulence caused by wind shear. Furthermore, strong wind shear due to tremendous changes both in wind speed and direction occurs at around 1.5 km, resulting in stronger local turbulence. To estimate the stratification over the sea and the stability of the boundary layer, the Bulk Richardson number R_B has been calculated using radiosonde measurement, defined in its usual form as [Stull, 2012]

$$R_{\mathrm{B}} = \frac{\dfrac{g}{\theta_v}\dfrac{\Delta\theta_v}{\Delta z}}{\left(\left(\dfrac{\Delta U}{\Delta z}\right)^2 + \left(\dfrac{\Delta V}{\Delta z}\right)^2\right)} \tag{2}$$

where g is the acceleration due to gravity and θ_v, U, V are the virtual potential temperature, northward and eastward horizontal velocity component, respectively.

Large value of R_{B} is related to relative higher thermal stability and/or weaker wind shear with less turbulent activity, while small value of R_{B} is related to relative lower thermal stability and/or stronger wind shear with stronger turbulent activities. The balance between shear production and buoyant dissipation of energy results in a critical flux Richardson number $R_e = 0.25$ and $R_{\mathrm{T}} = 1$, which may be used to develop a prognostic equation for the growth of the SBL. When $R_{\mathrm{B}} < R_e$, the instability of laminar flow may result in Kelvin-Helmholz (K-H), an unstable wave that feeds on the mean shear and can overturn to produce patches of turbulent mixing, but it is not guaranteed since a low R_{B} is a necessary but not sufficient condition for K-H. When $R_{\mathrm{B}} > R_{\mathrm{T}}$, the turbulent flow changes into laminar flow and results in dynamic and static stability (Rahn, et al., 2016). The profiles of R_{B} are presented in Fig. 7 with black lines. In most cases, the R_{B} is large at the LLJ nose because of the strong temperature gradient and the relatively small wind shear, implying suppressed turbulence and dynamically stable atmosphere at this level. Much smaller R_{B} in the shear zone below the jet indicates significant turbulence mixing because of large wind shear (Banta, et al., 2006). Similarly, despite the strong temperature gradient in the second inversion layer, the wind shear is sufficient to reduce the R_{B} below the critical Richardson value of R_e (Rogers, et al., 1996). The R_{B} is still large between the SBL height and 0.5 km, which may be the result of weak temperature gradient and weak wind shear effect. It is noted that the R_{B} is sensitive to the potential temperature fluctuation and thus singular value occurs discontinuously (Stull, 2012).

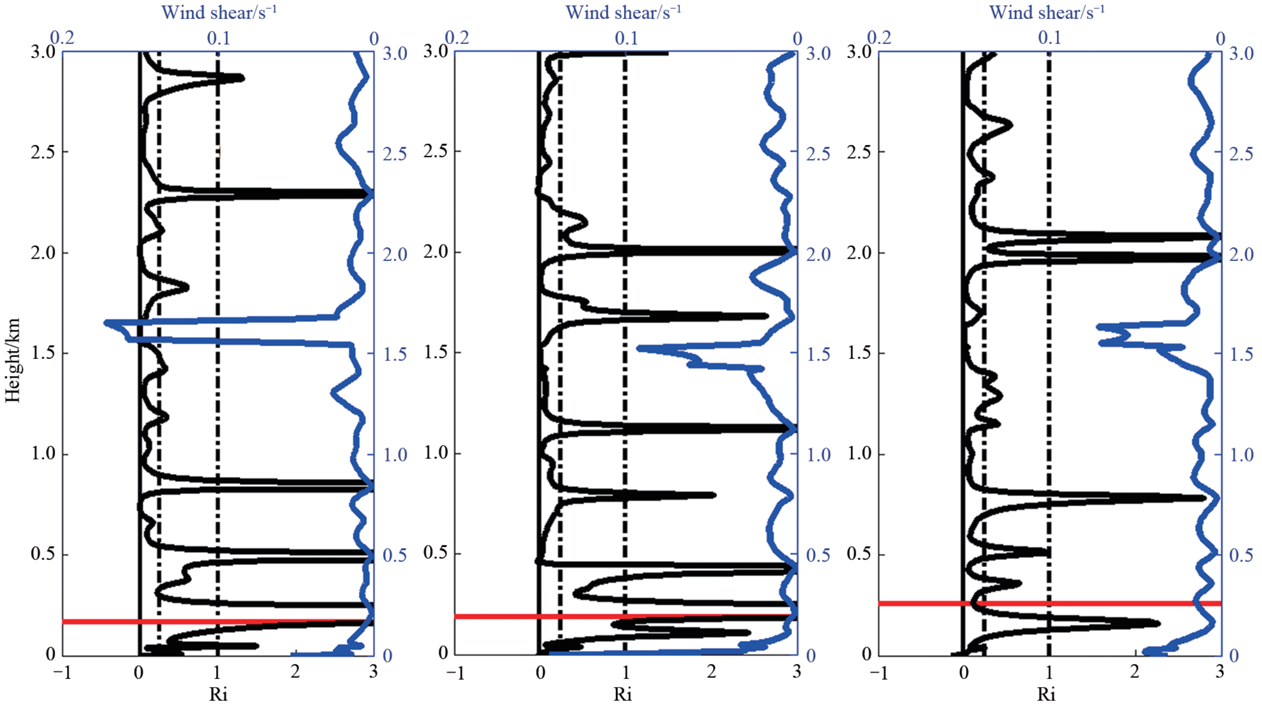

(a) 08:05 LST May 9, 2014 (b) 10:18 LST May 9, 2014 (c) 12:04 LST May 9, 2014

Fig.7 Profiles of vertical wind shear and Richardson number for 08:05, 10:18, 2:04 LST May 9, 2014 at corresponding voyage location, respectively, and the horizontal red lines are the MABL height derived from potential temperature profile characterization, the vertical black solid lines and dot lines represent $R_{\mathrm{B}} = 0$, $R_{\mathrm{B}} = 0.25$, $R_{\mathrm{B}} = 1$, respectively

3.3 Analysis of CDL vertically pointing mode measurement

In the following section, the CDL dataset measured from 07:42 LST May 9, 2014 to 20:57 LST May 9, 2014 are analyzed in detail. The voyage ship travels from 122°57' E, 36°28' N to 123°10' E, 36° 59' N during the observation period, and the specific cruise route of which is marked with red line in Fig. 1.

Fig. 8 (a) shows the time-height-intensity of SNR obtained from CDL vertically pointing mode (mode 2). Data below 120 m is not available because of the overlap effect. It is shown that there are two aerosol layers at around 0.7—1 km and 1.8—2.8 km before 10:00 LST. The lower layer was decoupled with the atmosphere below firstly, then gradually descended and mixed well. The higher layer has stronger intensity and thicker physical structure. It is hard to identify whether this strong intensity is due to the microphysical properties of aerosol particles or is due to the number density, but the contribution from swelling of the particles is presumably small since the radiosonde data showed relative humidity below 90% in this layer (Wulfmeyer, et al., 2000). Afterward, there are two aerosol layers at 0.8 —1.5 km and 1.7—3 km, respectively. The lower one has no obvious diurnal variation in height and thickness. In contrast, the higher one gradually descends from 2.5 km to 2 km, and the thickness also changes from 1 km to 0.3 km, which are consistent with the features shown in the profiles of relative humidity shown in Fig. 5. It is interesting to find that the sudden change of wind direction occurs between these two aerosol layers as well. The backward trajectory analysis based on the HYSPLIT model (Draxler, et al., 2003) from NOAA leads to the possible sources of the aerosol layers. The backward trajectories simulated by the HYSPLIT model in 12 height levels at 36.71°N, 123.11° E are presented in Fig. 9. The hourly air temperature and wind field distribution at different pressure levels (700 hPa, 800 hPa, 900 hPa and 1000 hPa) are shown in Fig. 10. On the basis of the trajectory and air temperature results, the air mass above 1 km keeps in a relative stationary condition in each height level and travels from warm land to cold sea. Therefore, the higher aerosol layer at 1.7—3 km may result from the warm advection from the Eurasian continent, consistent with the fact that the westerly wind dominates the wind field in these height levels. The air mass below 1 km gradually descends from northeast to southwest affected by high-pressure weather system. The lower aerosol layer at 0.8—1.5 km has different features like wind speed, relative humidity with the lower atmosphere. The existence of such a structure is not entirely unheard of (Rahn, et al., 2016a, Rahn, et al., 2016b). For this case, the wind acceleration in this region makes the vertical wind shear stronger so that the R_B reduced and favors shear instability that may induce KH instability and break down into turbulence. So different formation mechanism and sources of these two aerosol layers results in different characteristics. Furthermore, the SNR in the lower atmosphere is slightly lifting at afternoon, and the R_B at 14:08 is less than 0.25 in this region, suggesting that the atmospheric condition is more turbulent in this period. The sudden subsidence of SNR during 16:13—17:20 is the result of the reduction in laser energy.

The corresponding vertical velocity data has been corrected using ship motion correction algorithm described in previous literature (Zhai, et al., 2018). The vertical velocity time-height cross section is shown in Fig. 8 (b), where the positive value represents the updraft and vice versa. Quality control based on the SNR threshold method was used to exclude "bad value" due to weak aerosol backscatter signal. It can be found that the vertical velocity measured by CDL is small in clear sky between ±1 m/s. Downdraft is prevailing during observation period, which is consistent with the lower divergence controlled by the anticyclone system, but there is also small-scale updraft, especially at 10:00—13:00, implying that the dynamic structure of the atmosphere displays multiple scale characteristics. The strength of updrafts and downdrafts are slightly weaker amounted to about 0.3 m/s at the beginning and end of the measurement period, and stronger downdrafts occurs at around 13:00—18:00. It is noted that the continuous vertical motion can be seen in the upper aerosol layer, showing different turbulent characteristics compared within SBL.

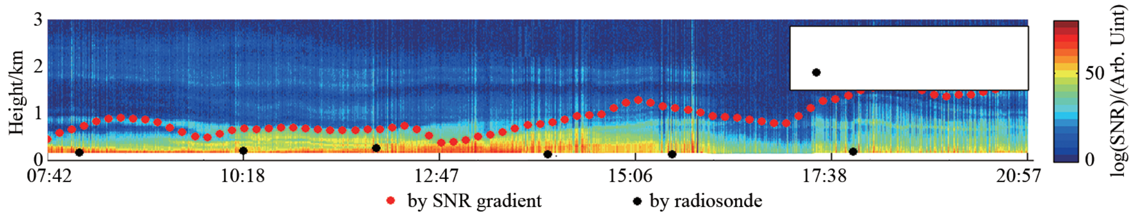

(a) Time-height-intensity

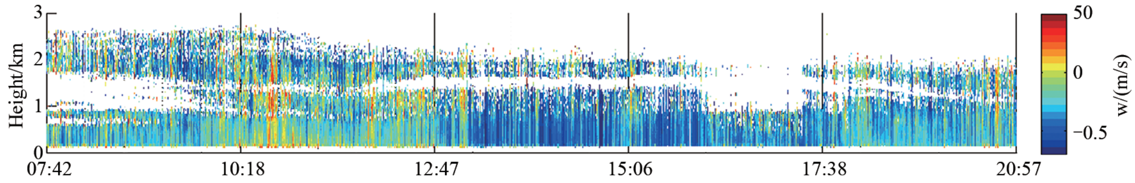

(b) corresponding vertical velocity data

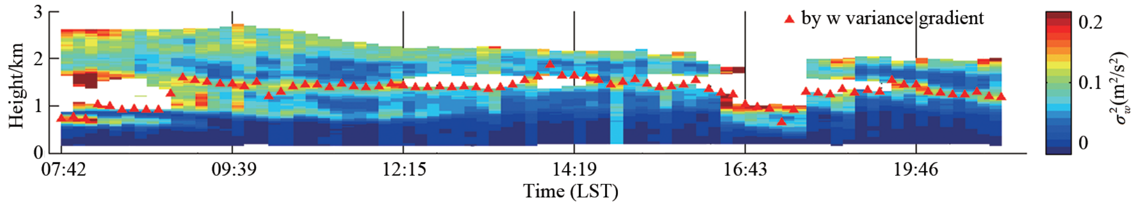

(c) corresponding vertical velocity variance data

Fig.8 Time-height-intensity of SNR and MABL height using SNR gradient method (red solid circle) and radiosonde potential temperature (black solid circle), corresponding vertical velocity data, corresponding vertical velocity variance data and MABL height using vertical velocity variance gradient method (red solid triangle)

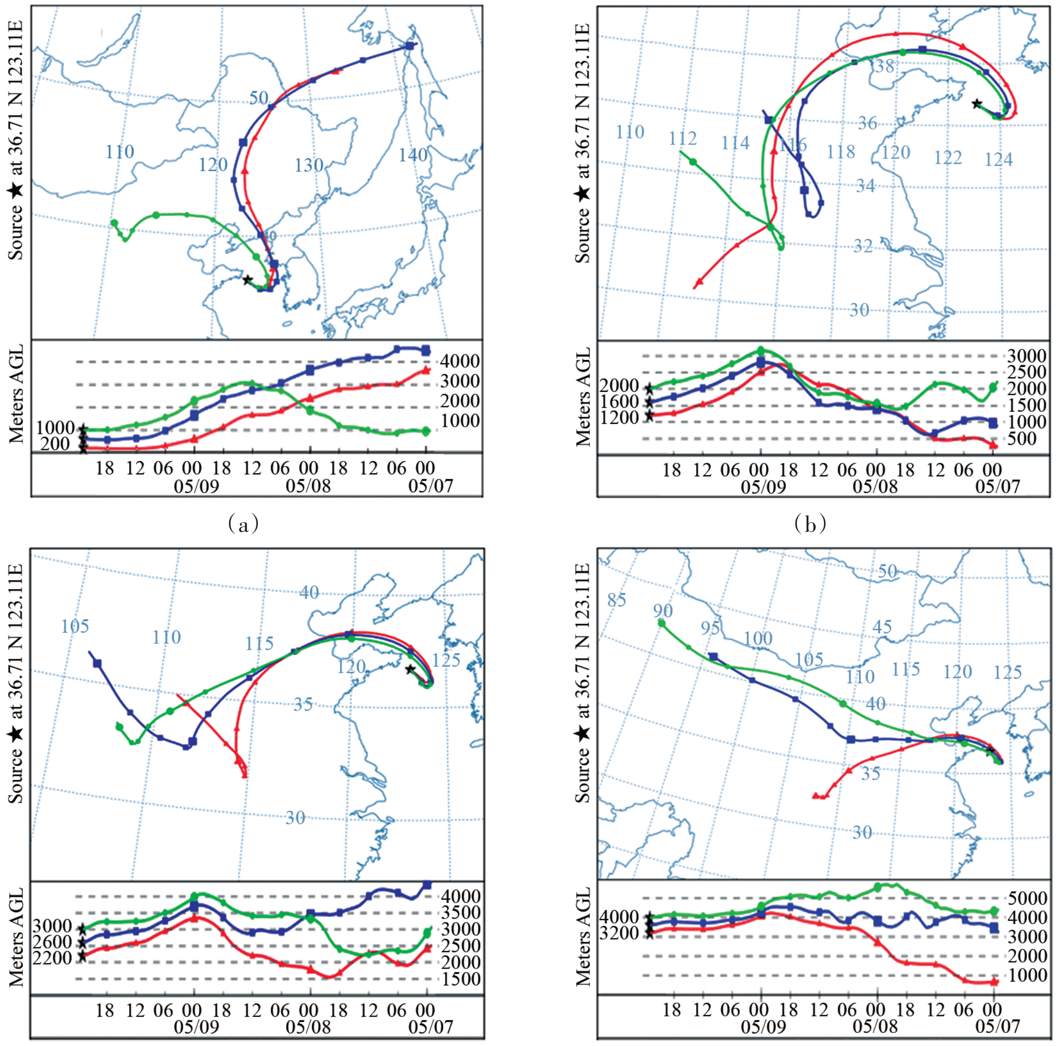

(a) (b)

(c) (d)

Fig.9 Backward trajectories ending at 23:00 LST May 9, 2014 at (a) 200 m (red line), 600 m (blue line), 1000 m (green line), (b) 1200 m (red line), 1600 m (blue line), 2000 m (green line), (c) 2200 m (red line), 2600 m (blue line), 3000 m (green line), (d) 3200 m (red line), 3600 m (blue line), 4000 m (green line) at observation location (36.71°N, 123.11°E) simulated by the HYSPLIT model

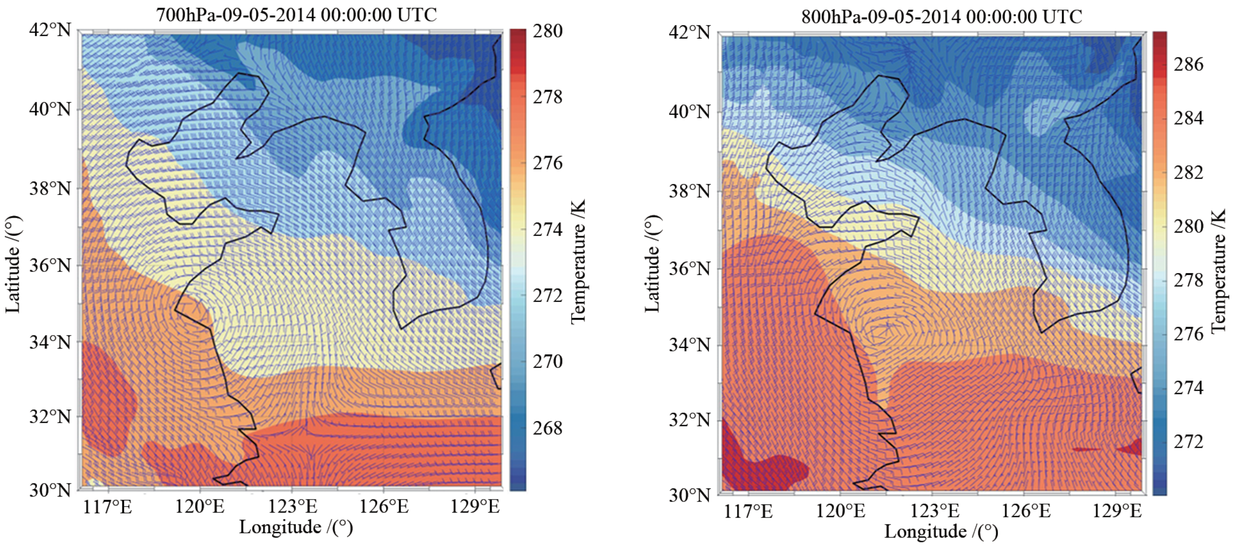

(a) 700 hPa (b) 800 hPa

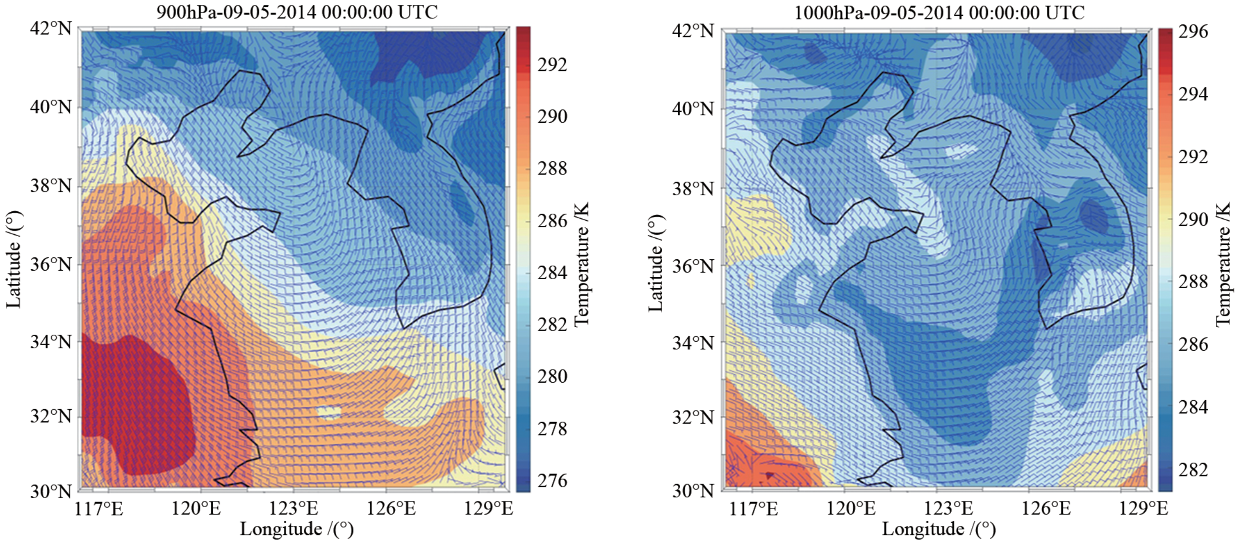

（c）900 hPa （d）1000 hPa

Fig.10 The distribution of wind vectors（barbs，m/s）and temperature（K）at 00 UTC May 9，2014 derived from the ECMWF ERA5 reanalysis dataset at 700 hPa，800 hPa，900 hPa and 1000 hPa.

The vertical velocity variance σ_w^2 can represent the atmospheric turbulence to some extent (Banta, et al., 2006, Tucker, et al., 2009). The estimation of σ_w^2 profile starts by creating a velocity time series from the data in each 30 m range gate in each 10 min zenith stare period. Noted that the total variance σ^2 includes both the atmospheric variance σ_w^2 and the instrument variance σ_{inst}^2, thus the resulting difference between σ^2 and σ_{inst}^2 gives the estimates of σ_w^2 (Lenschow, et al., 2000). Obviously, the stronger SNR below 1 km has weaker vertical velocity variance, which is consistent with large Bulk Richardson number. Furthermore, the upper aerosol layer with continuous vertical motion has stronger variance than the lower part of atmosphere.

4 RESULTS

4.1 MABL height retrieval and comparison

The height of the MABL Z_i is a common scaling variable that reflects the strength of the turbulence activity. Therefore, it is important to estimate this variable with high resolution and accuracy. However, the MABL height is more difficult to quantify for the stable than unstable regime, and there is no unique algorithm to determine the SBL top accurately without actual observations of the turbulence kinetic energy profile in the boundary layer (Liu, et al., 2010). One of the most common way to determine the Z_i is to locate the increase of virtual potential temperature in radiosonde profiles, which is marked with black solid circles in Fig. 8 (a). Furthermore, using active remote sensing, a higher temporal resolution of boundary layer data can be obtained, leading to better sampling statistics of the instantaneous boundary layer height. However, it is noted that the SBL height analysis by CDL is not possible when the SBL height is below 120 m. Since the boundary layer has higher aerosol concentrations than the free troposphere above, the first strong negative gradient in SNR is considered as the Z_i in some previous studies (Hennemuth, et al., 2006). In this paper, the SNR gradient method is firstly used to determine the Z_i, and the results are marked with black solid circles in Fig. 8 (a). The profiles of SNR (blue lines) and retrieved Z_i (horizontal blue lines) at corresponding radiosonde time are shown in Fig. 11. Table 1 lists the retrieved Z_i using different methods. It can be seen that the results from CDL and radiosonde are quite different due to the difference on Z_i definition and criterion. Specially, the Z_i from radiosonde virtual potential temperature is generally defined as the SBL height, while the Z_i from CDL SNR focuses on the aerosol concentration variation between boundary layer and free atmosphere, and sometimes is defined as the mixing height in SBL. But in this case, the lower aerosol layer complicates the issue and the deviation between the Z_i from CDL SNR and the defined SBL height based on potential temperature is evident.

Vertical velocity variance from CDL has also been used in boundary layer depth estimation. Lothon et al (Lothon, et al., 2006) estimated the mixing height in the unstable daytime CBL by searching for the lowest altitude where the σ^2 exceeds a large threshold values, which is strongly dependent on aerosol concentrations. Tucker et al (Tucker, et al., 2009) used the corrected vertical velocity variance σ_w^2 to define mixing height where the σ_w^2 drops below a specific threshold. Both of them are focused on CBL, and the availability in SBL condition is uncertain. In this study, by comparing the σ_w^2 profile with the radiosonde potential temperature data, it is found that the second inversion layer at around 1.5 km corresponds to the minima of the variance gradient or the first invalid value. It makes sense that mixing height can be identified using the turbulence difference between boundary layer and free atmosphere, which is similar with Tucker et al criterion [Tucker, et al., 2009]. According to this characteristic, the mixing height in SBL has been retrieved and shown in Fig. 8(c) marked with red triangles. Similarly, the profiles of σ_w^2 (black lines) and retrieved Z_i (horizontal black lines) at corresponding radiosonde time are shown in Fig. 11, which is also listed in Table 1. The difference of results from CDL SNR and σ_w^2 are also significant, and the Z_i from σ_w^2 is higher than SNR's. Interestingly, the Z_i retrieved from SNR gradient method corresponds to the height where the σ_w^2 suddenly increased in the lower atmosphere. It is not clear yet whether the SNR intensity is associated with the σ_w^2.

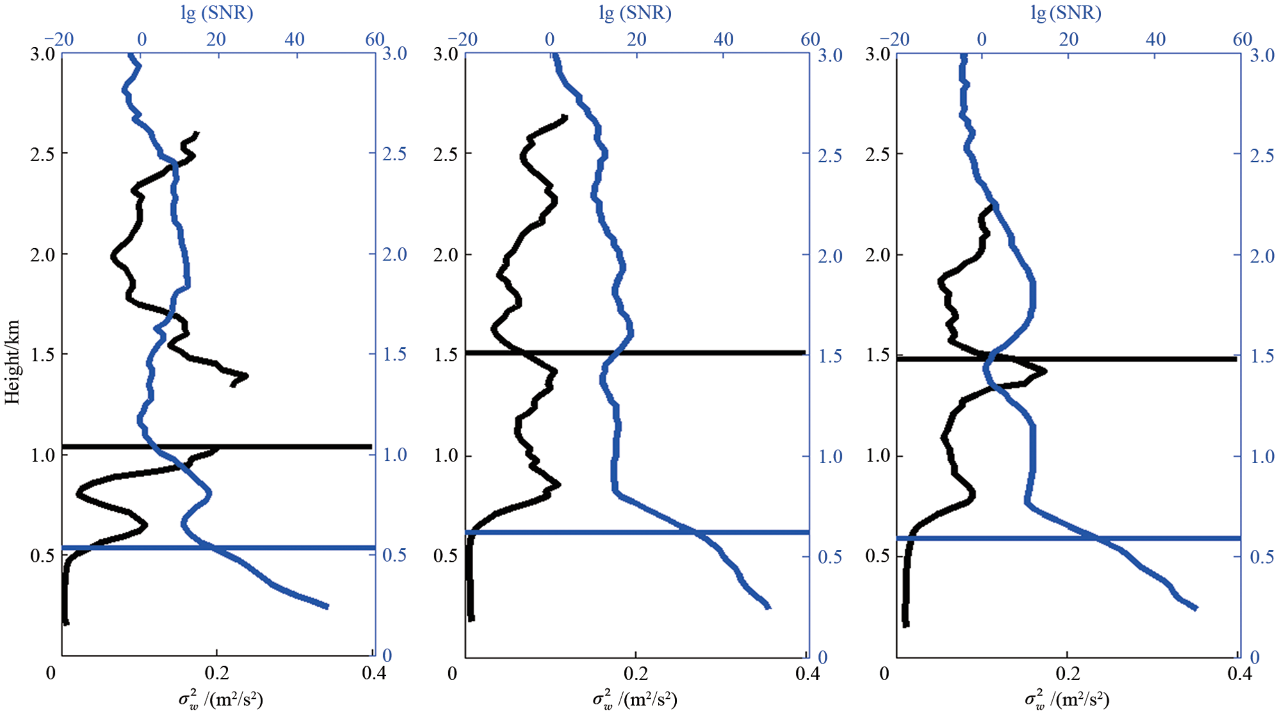

(a) 08:05 LST May 9, 2014 (b) 10:18 LST May 9, 2014 (c) 12:04 LST May 9, 2014

Fig.11 Profiles of vertical velocity variance (m²/s², black line) and SNR (blue line) for (a) 08:05 (b) 10:18, (c) 12:04 LST 9 May 2014 at corresponding voyage location, respectively, and the horizontal black and blue lines stand for MABL height retrieved from vertical velocity variance and SNR, respectively

Table 1 list of retrieved Z_i using different methods mentioned in this study

	08:05 LST May 9, 2014	10:18 LST May 9, 2014	12:04 LST May 9, 2014
Radiosonde potential temperature method	167 m	183 m	267 m
SNR gradient method	533 m	650 m	600 m
Vertical velocity variance method	1050 m	1550 m	1500 m

4.2 Determination of turbulence higher-order moments

The previous studies have discussed the higher-order velocity statistics within clear and cloud-topped convective boundary layer (CBL), and proved that higher-order moment statistics can provide useful information about the structure of turbulence in CBL [Lothon, et al., 2009]. Few studies have been focused on the higher-order vertical velocity statistics within the marine stable boundary layer. In this section, the variance, skewness and kurtosis of vertical velocity in SBL are retrieved at different time periods and compared with the previous studies.

In order to analyze the diurnal variation of these variables, three time periods are divided during the observation period and Fig. 12 shows the results during 07:42 to 12:57 LST May 9, 2014 period. Each variable is presented with and without taking into consideration the motion of the ship, and is a function of normalized height $Z_* = Z/Z_i$, where Z_i is the mixing height retrieved from σ_w^2 gradient method. The values below $0.2Z_*$ are not reliable and plotted. It can be shown that the variance has the maximum at $0.9Z_*$, which is different from the CBL observations with maximum at about $0.3Z_*$ to $0.4Z_*$ (Lenschow, et al., 2000). The correction for ship motion is significant and the difference (marked with blue dashed lines) decreases with height and is reasonable because the magnitude of the correction is more sensitive to smaller horizontal wind speed (Zhai, et al., 2018).

The skewness of vertical velocity, given by

$$S = \overline{w'^3} / \overline{w'^2}^{3/2} \tag{3}$$

where w' is the fluctuation from the mean vertical wind, S provides a measure of the asymmetry in the distribution of vertical velocity perturbations within the boundary layer.

A great of attention has been focused on the profiles of vertical velocity skewness exhibited with both the fair-weather convective boundary layer and the stratus-topped boundary layer. It is found that the sign of the skewness can indicate whether turbulence is driven by surface heating or cloud-top cooling (Hogan, et al., 2009). But for the SBL in this study, the turbulence is generated mainly by shear at the transition between the surface flow and the overlying synoptic flow. It can be found that the averaged skewness in each height is positive, indicating that strong narrow updrafts are surrounded by larger areas of weaker downdraft (Moyer, et al., 1991). The skewness of the lower part in Fig. 12 (below $0.4Z_*$, $0.4Z_*$, $0.6Z_*$, respectively), corresponding to small variance region, increases with the height and then decreases gradually until at around $0.9Z_*$—Z_*, finally increases up to $1.1Z_*$, and this is similar to surface-driven CBL cases that the skewness increases with height over the lower portion of the fair weather boundary layer but is essentially constant within the upper portion (Lenschow, et al., 1980, Lenschow, et al., 2000). It may be the result of shear-driven turbulence mechanism. That is, as the stability increases, there is an increase in the turbulence due to an increase in wind shear, then vertical mixing increases, stability decreases and the layer thus deepens, causing stronger upward transport of Turbulence Kinetic Energy (TKE).

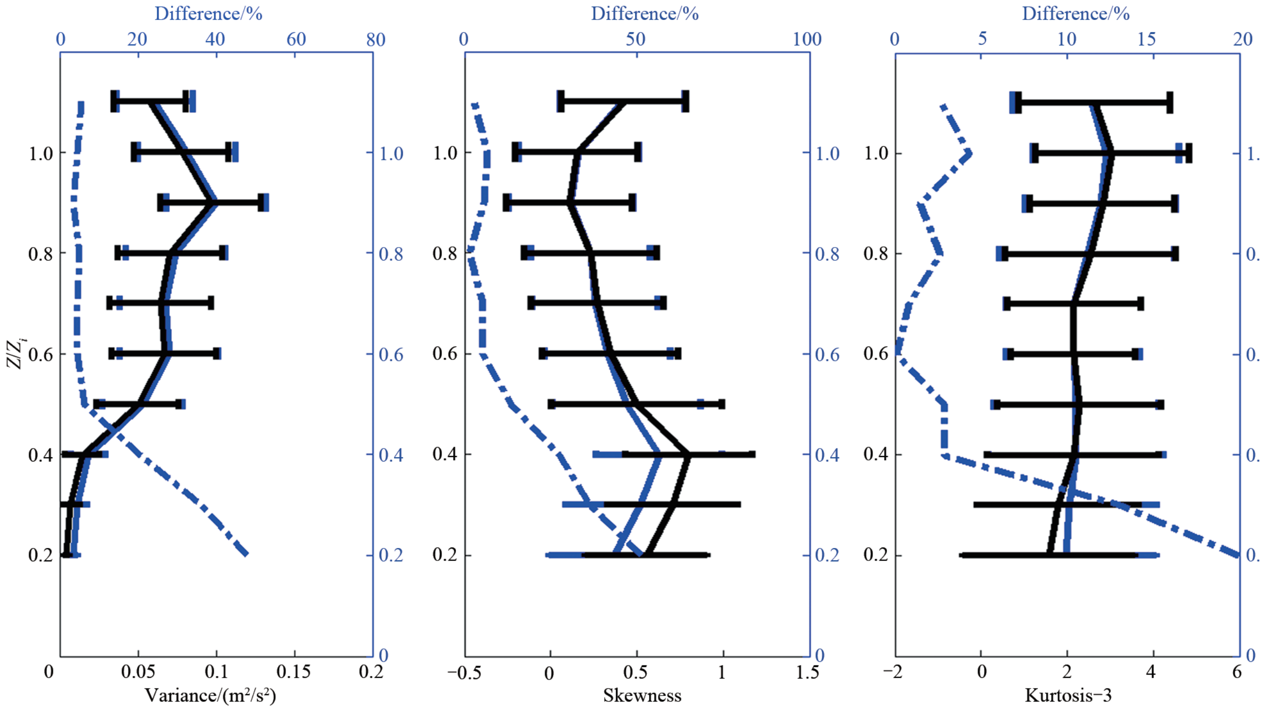

（a）Vertical velocity variance profile （b）corresponding skewness profile （c）corresponding kurtosis−3 profile

Fig.12 Vertical velocity variance profile obtained fromLidar from 07:42 to 12:57 LST May 9, 2014 with corresponding sampling error bars without (black line) and with (blue line) correction for motion of the ship, the blue dashed line stands for the difference between corrected and uncorrected vertical velocity variance

The kurtosis of vertical velocity is defined by

$$K = \overline{w'^4} / \overline{w'^2}^2 \tag{4}$$

K can represent whether the data are heavy-tailed or light-tailed relative to a normal distribution. Since normal distribution has a kurtosis of 3, Fig. 12 (c) shows $K - 3$ to make comparison with normal distribution. The results are in good agreement with the most shear LES results and previous observations (Lenschow, et al., 1980, Lenschow, et al., 2000, Sullivan, et al., 2008) showing a gradual increase within mixing height and a slight decrease above mixing height. Furthermore, the correction for ship's motion is less significant than variance and skewness's.

5 DISCUSSION AND CONCLUSION

Shipborne experimental investigation with OUC CDL in 2014 were carried out to study the structure of marine boundary layer in the Yellow Sea and to improve our understanding of MABL dynamic and thermal characteristics, turbulence and entrainment in the mid-latitude oceanic area. The performance of CDL was very reliable, confirming the feasibility of operating the lidar system in a routine manner on a moving platform. The highlights of the CDL include the flexible range resolution from 15 m to 60 m and relative high sampling rate of 4 Hz, which is useful for detection of small-scale turbulence feature and reduces the uncertainty in an averaged wind measurement. Ship motion turns out to be an important error source for the turbulence variables, so a motion correction method is firstly carried out to calibrate the horizontal and vertical wind profiles, the feasibility of which has been verified through the comparison experiment with radiosonde in the previous literature. The profiles of vertical velocity higher-order moments are also calculated after motion compensation, showing that correction for motion compensation are required and significant. A 16-hour continuous measurement of lidar SNR and vertical velocity profiles by CDL and corresponding 6 radiosonde datasets are analyzed. The vertical wind shear and *Ri* are also calculated to estimate the stratification over the sea and the stability of the boundary layer. The result reveals a complex three-layer structure of the lower troposphere, that is, below the first inversion layer, above the second inversion layer and between these two inversion layers, respectively. The lowest layer shows a typical stable boundary layer structure feature, consistent with negative sensible heat flux and negative sea-air temperature difference. Strong wind shear induced by low level jet occurs in this layer, and turbulence appears to be continuous, maintained by the strong wind shear production against the stability of downward-directed heat flux. However, an aerosol layer with an obvious abrupt in wind speed and relative humidity always appears within this layer. The existence of this structure may be due to the Kelvin-Helmholz instability. Specially, the wind acceleration in this region makes the vertical velocity wind shear stronger so that the R_B becomes reduced and favors shear instability that breaks down into turbulence. The top layer encounters a drastic change in wind direction compared with the other two layers, that is, the wind direction changes from westerly flow within the lower two layers to easterly flow within the top layer. On the basis of backward trajectory analysis of HYSPLIT model, it is found that the top layer travels from warm land to cold sea, so it may result from the warm advection from the Eurasian continent, consistent with the fact that westerly wind dominants the wind field in this height level. Different formation mechanism and sources of these two aerosol layers results in different characteristics. Downdraft is prevailing during observation period, but there is also small-scale updraft, implying that the dynamic structure of the atmosphere displays multiple scale characteristics. The vertical velocity variance σ_{w}^2 can represent the atmospheric turbulence to some extent. It can be seen that the weaker σ_{w}^2 is consistent with large Bulk Richardson number and shows atmospheric stability.

The MABL height is more difficult to quantify for the stable than unstable regime. Basically, the height of the first inversion layer is usually defined as the SBL height, and the height between the residual layer with nearly constant potential temperature and the free atmosphere is defined as the mixing height in SBL. In this paper, three methods based on potential temperature, SNR, σ_{w}^2 are introduced and compared, respectively. The SBL heights from potential temperature profile shown in Fig. 5—7 with horizontal red liens are less than 0.3 km with no distinct diurnal variation, showing the solar radiation is not the primary factor in affecting the SBL height. The Z_i from CDL SNR shown in Fig. 8 (a) with red solid dots are based on the aerosol concentration variation between the boundary layer and the free atmosphere, considering the first strong negative gradient in SNR as the boundary layer height. In this study, neither the SBL height derived from radiosonde potential temperature profiles nor the mixing height derived from vertical velocity variance shown in Fig. 8 (c) with red solid triangle are in agreement with the Z_i from CDL SNR gradient method because of different criterion, and the aerosol layer at 0.8—1.5 km may also complicate this issue, which makes the results retrieved from SNR gradient method ambiguous. By comparing the σ_{w}^2 with the potential temperature profile, it is found that the inversion layer between residual layer and residual layer corresponds to the minimum of the σ_{w}^2 gradient or the first SNR invalid value, making sense that mixing height can be identified using the σ_{w}^2 gradient method. The difference of the results from CDL SNR and σ_{w}^2 are also significant shown in Fig. 11. Interestingly, the Z_i retrieved from SNR gradient method corresponds to the height where the σ_{w}^2 suddenly increased in the lower atmosphere. More cases should be analyzed and validate the feasibility of the σ_{w}^2 gradient method in SBL.

Higher-order vertical velocity statistics within the marine stable boundary layer are investigated and compared with the previous studies in clear or cloud-topped CBL. The curves of σ_w^2 in different time periods show similar shape with a maximum value at $0.9Z_*$, which is different from CBL observation with maximum at around $0.3Z_*$~$0.4Z_*$. The skewness can indicate whether the turbulence is driven by surface heating or cloud-top cooling in CBL, but for SBL in this study, the turbulence is generated mainly by shear at the transition between the surface flow and the overlying synoptic flow. The averaged skewness is positive, indicating that the strong narrow updrafts are surrounded by large areas of weaker downdrafts. The shape of skewness profile in SBL is similar to surface-driven CBL cases that the skewness increases with height over the lower portion of the boundary layer but is essentially constant within the upper portion. The profiles of kurtosis are in good agreement with the most shear LES and previous observations, showing a gradual increase within the mixing height and a slight decrease above mixing height. Though we were able to investigate turbulence moments in the SBL, more research is required to analyze turbulent and transport processes in SBL and to understand its turbulent motion.

REFERENCES

Angevine W M, Hare J E, Fairall C W, Wolfe D E, Hill R J, Brewer W A and White A B. 2006. Structure and formation of the highly stable marine boundary layer over the Gulf of Maine. Journal of Geophysical Research: Atmospheres, 111D23

Banta R M, Pichugina Y L and Brewer W A 2006. Turbulent velocity-variance profiles in the stable boundary layer generated by a nocturnal low-level jet. Journal of the atmospheric sciences, 63(11), 2700-2719

Csanady G T. 1974. Equilibrium theory of the planetary boundary layer with an inversion lid. Boundary-Layer Meteorology, 6(1-2), 63-79

Draxler R R. 2011. Hysplit (hybrid single-particle lagrangian integrated trajectory) model access via NOAA ARL ready website. http:// ready. arl. noaa. gov/HYSPLIT. php

Eberhard W L, Cupp R E and Healy K R. 1989. Doppler lidar measurement of profiles of turbulence and momentum flux. Journal of Atmospheric and Oceanic Technology, 6(5), 809-819

Emeis S. 2018. Wind energy meteorology: atmospheric physics for wind power generation. Springer.

Garratt J R. 1987. The stably stratified internal boundary layer for steady and diurnally varying offshore flow. Boundary-Layer Meteorology, 38(4), 369-394

Hawley J G, Targ R, Henderson S W, Hale C P, Kavaya M J and Moerder D. 1993. Coherent launch-site atmospheric wind sounder: theory and experiment. Applied optics, 32(24), 4557-4568

Hogan R J, Grant A L, Illingworth A J, Pearson G N and O'Connor E J. 2009. Vertical velocity variance and skewness in clear and cloud-topped boundary layers as revealed by Doppler lidar. Quarterly Journal of the Royal Meteorological Society: A journal of the atmospheric sciences, applied meteorology and physical oceanography, 135(640), 635-643

Hennemuth B and Lammert A. 2006. Determination of the atmospheric boundary layer height from radiosonde and lidar backscatter. Boundary-Layer Meteorology, 120(1), 181-200

Lenschow D H, Wyngaard J C and Pennell W T. 1980. Mean-field and second-moment budgets in a baroclinic, convective boundary layer. Journal of the Atmospheric Sciences, 37(6), 1313-1326

Lenschow D H, Wulfmeyer V and Senff C. 2000. Measuring second-through fourth-order moments in noisy data. Journal of Atmospheric and Oceanic Technology, 17(10), 1330-1347

Liu S and Liang X Z. 2010. Observed diurnal cycle climatology of planetary boundary layer height. Journal of Climate, 23(21), 5790-5809

Lothon M, Lenschow D H and Mayor S D. 2006. Coherence and scale of vertical velocity in the convective boundary layer from a Doppler lidar. Boundary-layer meteorology, 121(3), 521-536

Lothon M, Lenschow D H and Mayor S D. 2009. Doppler lidar measurements of vertical velocity spectra in the convective planetary boundary layer. Boundary-layer meteorology, 132(2), 205-226

Mitsuta Y and Fujitani T. 1974. Direct measurement of turbulent fluxes on a cruising ship. Boundary-Layer Meteorology, 6(1-2), 203-217.

Moyer K A and Young G S. 1991. Observations of vertical velocity skewness within the marine stratocumulus-topped boundary layer. Journal of the Atmospheric Sciences, 48(3), 403-410

Rahn D A, Parish T R and Leon D. 2016. Observations of large wind shear above the marine boundary layer near Point Buchon, California. Journal of the Atmospheric Sciences, 73(8), 3059-3077

Rocers D P, Johnson D W and Friehe C A. 1995. The stable internal boundary layer over a coastal sea. Part I: Airborne measurements of the mean and turbulence structure. Journal of the atmospheric sciences, 52(6), 667-683

Smedman A S, Bergström H and Grisogono B. 1997. Evolution of stable internal boundary layers over a cold sea. Journal of Geophysical Research: Oceans, 102(C1), 1091-1099

Strauch R G, Merritt D A, Moran K P, Earnshaw K B and De Kamp D V. 1984. The Colorado wind-profiling network. Journal of Atmospheric and Oceanic Technology, 1(1), 37-49

Stull R B. 2012. An introduction to boundary layer meteorology (Vol. 13. Springer Science & Business Media

Sullivan P P and Patton E G. 2008. 11B. 5 A Highly Parallel Algorithm For Turbulence Simulations In Planetary Boundary Layers: Results With Meshes Up To 10243

Tucker S C, Senff C J, Weickmann A M, Brewer W A, Banta R M, Sandberg S P and Hardesty R M. 2009. Doppler lidar estimation of mixing height using turbulence, shear, and aerosol profiles. Journal of Atmospheric and Oceanic Technology, 26(4), 673-688

Wulfmeyer V and Feingold G. 2000. On the relationship between relative humidity and particle backscattering coefficient in the marine boundary layer determined with differential absorption lidar. Journal of Geophysical Research: Atmospheres, 105(D4), 4729-4741

Wulfmeyer V and Janjić T. 2005. Twenty-four-hour observations of the marine boundary layer using shipborne NOAA high-resolution Doppler lidar. Journal of Applied Meteorology, 44(11), 1723-1744.

Wu S, Liu B, Liu J, Zhai X, Feng C, Wang G and Gallacher D. 2016. Wind turbine wake visualization and characteristics analysis by Doppler lidar. Optics Express, 24(10), A762-A780

Zhai X, Wu S, Liu B, Song X and Yin J. 2018. Shipborne Wind Measurement and Motion-induced Error Correction of a Coherent Doppler lidar over the Yellow Sea in 2014, Atmos. Meas. Tech., 11, 1313-1331